Phys. Med. Biol. **45** (2000) 3627–3641. Printed in the UK PII: S0031-9155(00)13959-4

# Depth scanning for a conformal ion beam treatment of deep seated tumours

Uli Weber, Wolfgang Becher and Gerhard Kraft
Gesellschaft für Schwerionenforschung, Biophysik, Planckstraße 1, 64291 Darmstadt, Germany

Received 16 May 2000

**Abstract.** Only target-conformal treatment allows one to exploit the advantages of ion beams (the increased dose and high biological efficiency at the end of the particle range) to a maximum extent. Up to now, target-conformal treatments such as spot scanning or intensity-controlled raster scanning have used fast magnetic lateral deflection in one or two directions perpendicular to the beam axis and a slow range variation in the longitudinal axis by active or passive energy variation. The present paper describes a new method for conformal irradiation with a fast intensity-controlled longitudinal scan in the beam direction, called 'depth scanning'. Its advantages and disadvantages will be discussed. First experimental results from depth scanning will be presented.

## 1. Introduction

Extremely target-conformal treatment with protons or heavy ions offers the possibility of sparing the normal healthy tissue around the target volume to a maximum extent from excessive radiation, and of reducing the unavoidable dose in the entrance channel to a minimum. In addition, critical structures close to or even within the target volume can be spared by producing steep dose gradients between tumour and critical structures. Thus, the risk of acute and late toxicity of healthy tissue can be reduced.

In very modern facilities for ion beam therapy such as PSI in Villingen (Pedroni *et al* 1995) and GSI in Darmstadt (Kraft 1998, Debus *et al* 2000) the dose is conformed to the tumour by beam scanning. In this treatment technique, the target volume is divided into slices of equal particle range and each slice is treated by scanning the beam laterally either in one direction (for the proton beam at Villigen) or in two directions (for the carbon beam at Darmstadt) over each slice. In both cases the slice to be treated is covered by a net of pixels that have to be filled by a definite but varying particle fluence according to the dose necessary to produce a homogeneous dose or biological effect. When the irradiation of one slice is finished the energy is reduced by the accelerator or by passive absorber systems and the same procedure starts for the next slice. This elegant scanning technique (Goitein 1983, Haberer *et al* 1993) yields a dose conformity with the target volume that cannot be reached by conventional ion beam application techniques using bolus and collimator (Chu *et al* 1993). However, raster scanning described above requires an expensive construction and a very fast and complicated control system.

It is evident from recent experience with proton therapy facilities that a rotating gantry is very advantageous for a dedicated cancer therapy facility, where a large spectrum of tumour sites is expected, but, due to the large acceptance required of the last bending magnet of a gantry with an integrated raster scanning system, such a gantry would have an estimated weight of

0031-9155/00/123627+15$30.00  

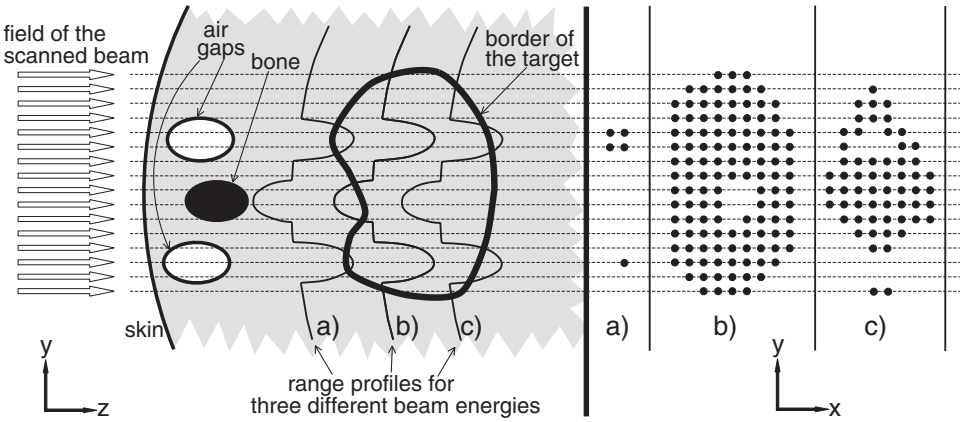


**Figure 1.** *Left part*, schematic drawing of three range profiles (a), (b) and (c) of stopping particles for three different energies selected from many more energies that are needed for a complete 3D-conformal irradiation. The strong bending of these slices is caused by density inhomogeneities such as air gaps and bones; the residual part of the body is assumed to be homogeneous for this drawing. Only the pixels of the slices within the target volume (tumour) are irradiated. Therefore, the pixel patterns show holes or small isolated groups as can be seen in the *right part*, which shows the same slices (a), (b) and (c) from a beams eye view. In contrast to the transversal slices, the longitudinal lines (in beam direction) within the tumour are normally not interrupted, which can also be seen in the left part of the drawing.

several hundred tons (Groß *et al* 1998). Another necessary component for fast lateral scanning systems is an equivalently fast monitor and a control system that measures the beam's position at each pixel and kicks off the beam extraction of the accelerator in case of larger deviations. This requires extremely fast and carefully designed electronics, as realized at GSI (Badura *et al* 2000). A further crucial point making raster scanning complicated is the division of the treatment volume into slices according to equal particle energy. Due to the inhomogeneous density of human bodies, a field scanned with a fixed particle energy does not yield a plane slice of constant range. Therefore, small volumes of high or low density—for instance those caused by bones or air gaps—form scanning patterns with isolated groups of very few beam spots or patterns having holes within (see figure 1). Thus the beam cannot be regularly moved over the slice and the beam's path becomes increasingly complex and frequently interrupted.

It is the scope of this paper to test an alternative beam application technique yielding the same conformity as a raster scan system but requiring a less expensive construction and control system. Starting from the problem of complicated and frequently interrupted patterns of the raster scanner (see above), it was discovered that if the target volume is viewed along a line parallel to the beam direction, the intersection of this line and the target volume is not intersected in the majority of cases (see section 3.4). The inhomogeneous density in the body stretches the line but does not interrupt it (see figure 1). Therefore, we examined whether is it possible to perform fast longitudinal scanning along a series of lines parallel to the beam direction. This scanning in the beam direction is intended to shift the Bragg maximum continuously along the lines with a velocity up to 50 cm $s^{-1}$.

Because a fast and continuous energy variation cannot directly be generated with a cyclotron or synchrotron, an absorber of variable thickness is used to shift the Bragg peak, while the accelerator is adjusted to a fixed energy corresponding to the deepest point of the target volume. The variation of the thickness of the absorber is controlled in real time by the intensity of the beam, in order to produce a well defined dose along the scanned lines.

This feedback system measuring the beam intensity continuously is essential for this technique and differs from standard techniques in particle therapy using absorbers of variable thickness. Wedge absorbers and range shifters—commonly installed in facilities for proton or heavy ion therapy—have to our knowledge not been used for fast continuous energy variation controlled by the beam intensity. Though so-called modulator wheels perform a fast continuous energy variation, the range of the variation of thickness is fixed for these devices. Therefore, modulator wheels cannot be used for our longitudinal scanning technique. A synopsis of devices for energy variation in particle therapy and some relevant publications were compiled by Chu *et al* (1993).

The following sections of this article explain the principles of the new technique for fast longitudinal scanning—so-called depth scanning—and present two methods for producing 3D-conformal irradiation with depth scanning. We also describe experiments proving the feasibility of depth scanning for the one dimensional and three dimensional case. This depth scanning technique has been submitted to the German and European patent office (Kraft and Weber 1998).

## 2. Material and methods

### *2.1. The principle of depth scanning*

For depth scanning the target volume is divided into cylinders ($C_i$) in which the Bragg peak is moved along the central axis with position ($x_i$, $y_i$) (see figure 2). Superimposing a series of $N_i$ beams with identical transversal position ($x_i$, $y_i$) and different Bragg peak positions (energies) an individual spread-out Bragg peak can be produced, that fills the appropriate cylinder $C_i$. In order to produce a smooth depth dose profile (in the longitudinal direction) the distances of these peak positions $z_{ij}$ ($j = 1, \ldots, N_i$) have to be much smaller than the width of the Bragg peak. Because the transverse beam profile is Gaussian from the accelerator, the necessary lateral overlap from one to the next cylinder can be achieved easily. If the distance between the cylinders is smaller than $0.7 \times$FWHM of the beam a completely homogeneous dose distribution can be achieved.

Because it is not possible to change the energy from the accelerator within milliseconds a fast mechanical system is required for moving the Bragg peak along the central axis of the cylinders. For this purpose a double wedge system is mounted on two linear motors driven by a control system that includes an ionization chamber as particle monitor. The main feature of the scanning system is to ensure that a pre-calculated number $n_{ij}$ of particles is applied to each pixel ($x_i$, $y_i$, $z_{ij}$). Therefore, a real time control system measures continuously the beam intensity (particle rate) and compensates its unavoidable fluctuations. The control system triggers the linear motor to move to the next pixel after the pre-calculated amount of particles has been deposited. The technical realization of this system is described in section 2.2.

Generally, the particle numbers $n_{ij}$ are much higher for the distal (deepest) pixels than for the proximal pixels (lowest depth), because the proximal part of the target volume is pre-irradiated to a large extent due to the irradiation of the distal part. This requires a large dynamic range for the drives. Available dose optimization algorithms (Krämer 2000) can be used for the calculation of the numbers $n_{ij}$.

*2.1.1. Three dimensional irradiation with the depth scanner.* Additionally, in order to produce a complete 3D scan with a conformal dose distribution, the dose maximum of the beam has to be moved in the other two dimensions (of second and third order) to change the $x$, $y$-position of the beam from cylinder to cylinder (see also figure 2). These scanning

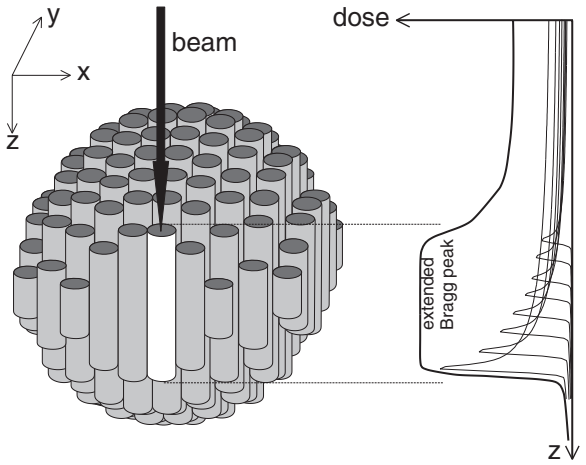


**Figure 2.** Spherical target volume divided in a series of cylinders $C_i$. Each cylinder is filled with a spread-out Bragg peak composed of many pencil beams which are shifted differently in depth by a fast wedge absorber system. The drawing shows cylinders having a sharp border, but in reality the spread-out Bragg peaks have a Gaussian lateral dose profile with a FWHM larger than the lateral distance of the cylinders, which guarantees a smooth lateral superposition.

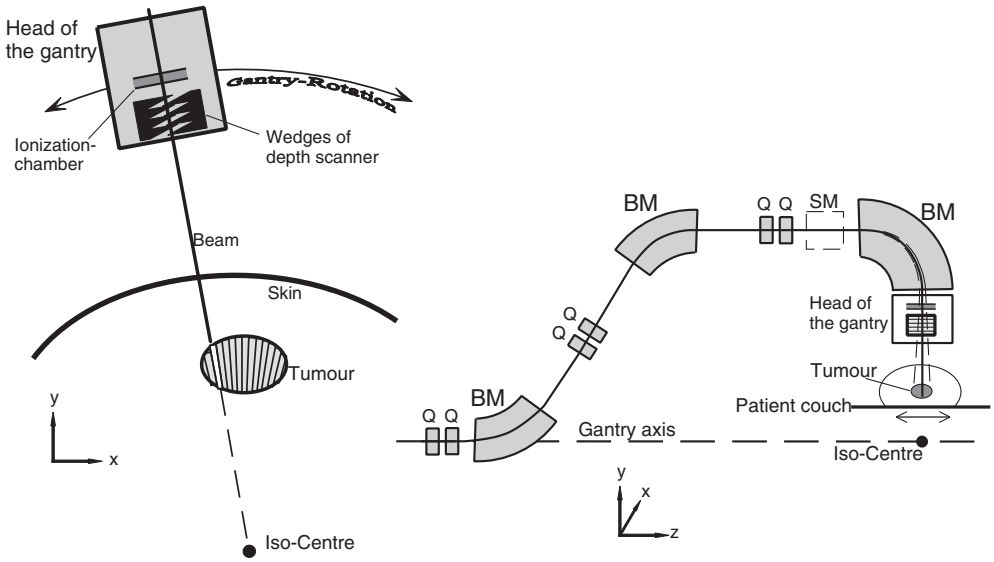


**Figure 3.** Schematic drawing of the depth scanner mounted in the head of a gantry (*left part*, viewed parallel to the gantry axis; *right part*, viewed perpendicularly to the gantry axis). For a slow beam scanning (second order) in the axial direction a sweeping magnet (SM) could be installed between the last quadrupoles (Q) and the last bending magnet (BM). Alternatively, the patient couch could be moved in the axial direction. The slowest motion of the beam (third order) is achieved by a stepwise rotation of the gantry with an iso-centre that is far behind the target volume in order to yield nearly parallel cylinders in the target.

directions are orthogonal to the beam direction which is the fastest scanning direction (of first order) as described before. In this section two possibilities are presented where the slower

scanning in the direction of second or third order can be realized with the use of a rotating gantry system (see figure 3). Both techniques allow a fully 3D-target-conformal irradiation in combination with depth scanning.

(I) The first technique combines a slow scanning (second order) of the beam in the axial direction and a very slow rotation of the gantry (third order) in the radial direction. The axial scan can be realized by using the last bending magnet of the gantry as a slow sweeping magnet or by using a separate small sweeping magnet. Due to the only one-dimensional magnetic scanning, the last bending magnet can have a smaller aperture and weight compared to the bending magnet of a gantry for transverse raster scanning, where the beam has to be scanned two-dimensionally through the last bending magnet (Pavlovic 1997).

(II) A purely mechanical solution is achieved by moving the patient couch slowly ($v < 10$ mm s$^{-1}$) parallel to the gantry axis (second order) and by very slowly rotating the gantry (third order).

Solution I is similar to a concept presented by the company IBA (Jongen *et al* 1991), with the main difference that the depth scanning of the IBA concept is performed with a fast rotating energy absorber of constant angular velocity. In comparison to the rotating absorber, however, the intensity controlled depth scanning system described in this paper is more flexible, because extended Bragg peaks of arbitrary shape and extension can be produced.

Due to the rotation of a gantry the individual cylinders are not exactly parallel for both solutions (I and II), but using a small correction for the radius this technique can be treated equivalently to a 3D scan in Cartesian directions. A positive side-effect of the non-parallel beams is a lower dose in the normal tissue in front of the tumour.

### *2.2. Technical realization of depth scanner*

*2.2.1. The multi-wedge system.* A critical point of depth scanning is a sufficiently high velocity and acceleration of the displacement of the Bragg peak. Therefore, the gradient of the absorber wedges has to be high enough. Figure 4 (right side) shows a pair of wedges made of Plexiglas (PMMA) that have a high effective gradient of roughly 1.9, defined as the ratio of the displacement of the Bragg peak of the beam passing through the absorber to the transverse displacement of the wedges. However, these wedges cause an undesired energy spread of the beam, because the beam is always broadened by multiple scattering. Due to the high geometrical gradient of the wedges (0.8) the overall path length of the particles in the material is not homogenous. This effect is also illustrated in figure 4.

In order to avoid this effect, a system of $2 \times 5$ (or more) stacked single wedges was designed (see figure 4, left side). Because of the lower geometric gradient of the single wedges (0.158) the energy spreading is reduced by a factor of five. Using the density conversion factor 1.165 for PMMA to water (Jacob 1997) the effective gradient of the complete wedge system can be calculated as

$$g_{\text{eff}} = 2 \times 5 \times 0.158 \times 1.165 = 1.845. \tag{1}$$

Plexiglas was chosen for the wedges, because it can be considered as water-equivalent and simplifies the treatment planning.

*2.2.2. The drives.* As described in section 2.1 the wedges are moved in accordance with the measured beam intensity $I(t)$. Therefore, the acceleration of the drives has to be high enough to compensate the fluctuations of beam intensity. In order to keep the velocity

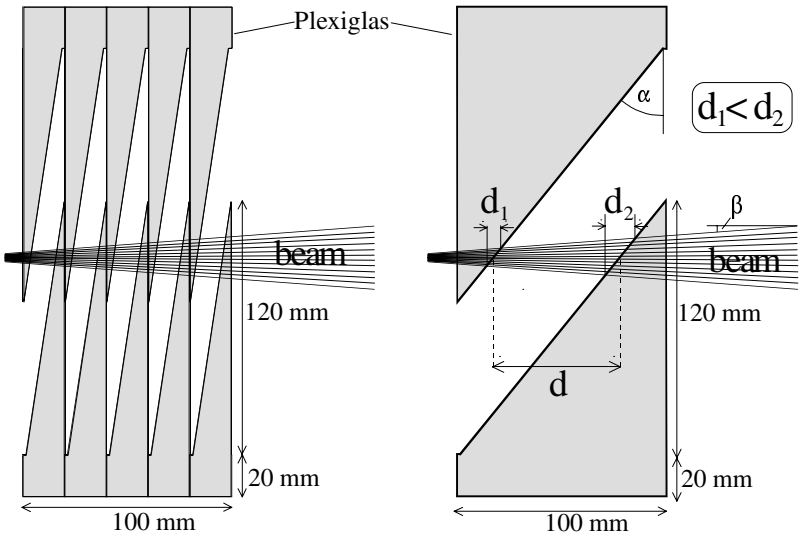


**Figure 4.** *Left side*, multi-wedge system used for the depth scanner with a high effective gradient. *Right side*, the single wedges have the same (effective) gradient as the multi-wedges, but due to the unavoidable widening of the beam the undesired energy spreading of the beam is much larger than for the multi-wedges. For reasons of elucidation the beam widening is exaggerated in the drawing. The energy spreading is induced by the non-uniform longitudinal beam displacement by the wedges. Due to the lateral widening of the beam (with angle $\beta$), the variance of the longitudinal beam displacement $d_1$ of the first wedge is not completely compensated by the second wedge ($d_2 > d_1$). The total variance of the single wedges can be estimated by $d_2 - d_1 \approx d \tan\alpha \tan\beta$. For thinner multi-wedges (left) the total variance is five times smaller: $5(d_2 - d_1)_{\text{small wedges}} \approx 5(d/5)(\tan\alpha/5)\tan\beta \approx 0.2d \tan\alpha \tan\beta$.

and acceleration of the absorber in a realistic range, a wedge absorber with a high effective gradient (see section 2.2.1) is used. Using such a wedge system and assuming a minimum spill length of 2–4 s, a maximum length of the extended Bragg peak of 15 cm and a desired accuracy of 3% for the depth dose profile, the requirements for the drive are as follows:

velocity, $v_{\max}$: 1–2 m s$^{-1}$

acceleration, $a_{\max}$: 20–30 m s$^{-2}$

precision of the drive: 100–200 $\mu$m

time constant of the controlling electronic: $<$1 ms.

These values result from a dynamic simulation of the system assuming a typical time structure of the beam extraction (see also section 3.1). For a cyclotron accelerator having a much smoother extraction profile in time these limits can even be reduced.

Standard electromechanical drives cannot fulfil these requirements, because they are too slow or not precise enough. For the realization of the depth scanner a drive with two linear motors was chosen, where the motors glide on a thin air cushion in opposite direction (Dreifke 1997). The whole motor moves on the stator like a magnetic monorail and carries the wedges (see figure 5). This drive easily fulfil the requirements specified above. Using an optical linear scale to control the drive the positioning precision is about 20 $\mu$m, the maximum velocity is 2 m s$^{-1}$ and the maximum acceleration with the load of the wedges is about 25 m s$^{-2}$.

For a three-dimensional scanning experiment at a fixed horizontal beam line (without gantry), two more stepper drives (standard technique) were installed in order to move the target

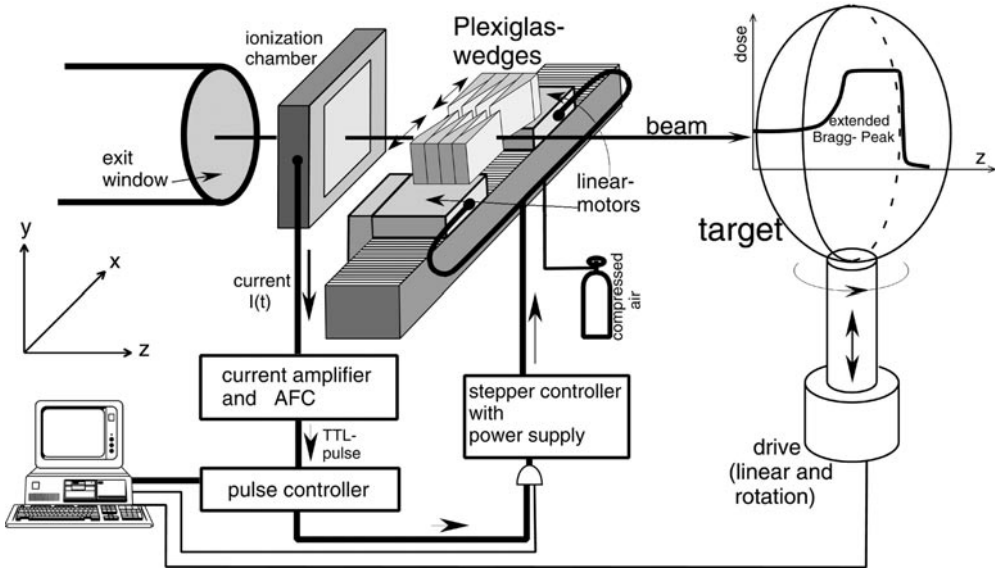


**Figure 5.** Depth scanning system with two multi-wedges mounted on two drives. For 3D scanning two additional drives (vertical translation and rotation) were installed to allow the movement of the target. The control system consists of an ionization chamber as particle monitor, a current amplifier with an amplitude-to-frequency converter (AFC), a pulse and stepper controller and a PC.

along the $y$ axis and to turn it around the $y$ axis (see figure 5). This was intended to simulate the scanning in the two remaining lateral dimensions. In these experiments, the rotation of the target is equivalent to a gantry rotation, while the translation in height corresponds to the slow scanning of the beam or to the slow translation of the patient (see section 2.1.1).

*2.2.3. The control system and its operation.* In our experiments the beam intensity is measured with a thin parallel plate ionization chamber producing a current proportional to the particle rate of the beam. The current is converted into a voltage by a fast and sensitive current amplifier (Keithley 428). Using an amplitude to frequency converter (AFC) the amplified signal is converted to TTL pulses. Thus, the feedback system produces TTL pulses with a rate proportional to the flux of ions passing through the chamber. The absolute proportionality factor $f$ depends on the species of the particles, the energy loss in the gas of the ionization chamber and the sensitivity of the amplifier. Calibration of this system yields typical values for $f$ of 200 particles per TTL pulse. The delay of the electronics and the ionization chamber (drift time) is about 200 $\mu$s.

The TTL pulse signal is fed into a special pulse controller, which is the interface between the intensity measuring system and the stepper controller for the drive (see also figure 5). Receiving a TTL pulse from the pulse controller the stepper controller changes the phase of the currents for the drive and the two motors move in opposition by one step of 20 $\mu$m shifting the Bragg peak $g_{\mathrm{eff}} \times 20$ $\mu$m in the negative beam direction. This pulse controller developed at GSI is a variable pulse rate divider. It has a large memory where several lists of numbers $n_{ij}$ ($j = 1, \ldots, N_i$) can be stored for the various cylinders $\mathrm{C}_i$ (see section 2.1). These numbers are proportional to the particle numbers of the $N_j$ beams to be superimposed.

In order to produce the individual extended Bragg peak for a cylinder $\mathrm{C}_i$, the $i$th list is activated in the pulse controller. When the beam is switched on, the stepper controller receives

the first TTL pulse from the pulse controller after the $n_{i,1}$th pulse comes from the AFC. The second pulse is received after the next $n_{i,2}$ AFC pulses, and so on. In this way the Bragg peak is stepwise shifted and superimposed to obtain the desired extended Bragg peak. A typical particle rate of the beam is about $10^8$ $s^{-1}$ and the step rate of the motors varies from 100 to 50 000 $s^{-1}$. So the motors perform a quasi-continuous movement but with a highly fluctuating velocity caused by the time structure of the beam intensity. When the last step for the cylinder is reached, the beam is switched off in less than 200 $\mu$s. The total number of particles used for the extended Bragg peak of cylinder $C_i$ is

$$M_i = f \sum_{j=1,\ldots,N_i} n_{ij}. \tag{2}$$

In practice a list has a typical length of 500–8000 elements and the pulse controller can store some hundred lists. Obviously the counting of particles described above is idealized because the control system has a delay and the intensity measuring system has a limited accuracy (3%), but these technical deviations are small and the desired accuracy can be obtained (see section 3).

In order to produce a three-dimensional irradiation a series of one-dimensional depth scans has to be overlaid (see figure 2). Therefore, after a depth scan is finished the target has to be shifted to the next position and the linear motors have to be moved to a new starting position for the next depth scan and the next list of numbers in the pulse controller has to be activated. When all lists are executed the complete 3D irradiation is finished.

In the experiment, the PC was used to transfer the list data coming from the dose optimization into the pulse controller. Furthermore the PC executes the move to the start positions $s_i^0$ of the wedges before performing the depth scan. Therefore, a Parker AT6400 PC card is connected to the stepper controller. In order to produce a three-dimensional scan the PC card also controls the stepper drives for the moves in the $y$ direction and the rotations around the $y$ axis (see section 2.1.1).

The complete process of a 3D scan with the depth scanner can be summarized as follows:

(a) Dose planning and optimization yield the numbers $n_{ij}$ of particles to be stopped at the pixels $z_{ij}$ and the start positions of the wedges $s_i^0$.

(b) The PC transfers the lists with the numbers $n_{ij}$ into the pulse controller. The first list is activated.

(c) Controlled by the PC card the target and the linear motors with the wedges are moved to their start positions.

(d) The beam (spill) is started with an energy (e.g. 250 MeV $u^{-1}$) constant for the complete irradiation.

(e) Depth scan: shifting the wedges stepwise a series of beams ($j = 1, \ldots, N_i$) with different Bragg peak positions $z_{ij}$ and $fn_{ij}$ particles is superimposed, in order to fill the cylinder $C_i$ with the desired extended Bragg peak.

(f) The extraction of the beam is aborted when the last step ($j = N_i$) of the cylinder is reached.

(g) In order to produce a three-dimensional irradiation the target is shifted or rotated to the position for the next cylinder ($i \rightarrow i+1$) and the linear motors are moved to a new starting position $s_i^0$. Then the procedure continues at step (d).

(h) When all cylinders $C_i$ are filled the 3D irradiation is completed.

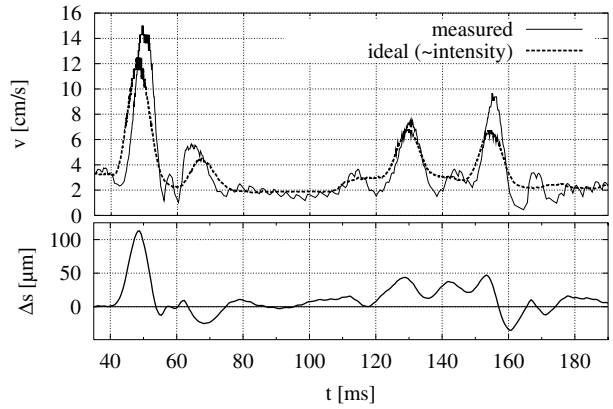


**Figure 6.** Measurement of the velocity $v(t)$ of the drive in comparison to the ideal velocity, being proportional to the beam intensity $I(t)$. The graph only contains a small but typical part of the whole extraction phase (spill). The lower part of the diagram shows the deviation $\Delta s(t)$ of the actual measured position from the ideal position.

## 3. Experiments and results

### *3.1. Dynamics of the drive*

Obviously, the performance of the drives determines the accuracy of the depth scanning system. The static precision and reproducibility of the drives is in the range of a few micrometres. This does not effect the dose accuracy of the system. More critical is the dynamic accuracy of the drives during the movement, i.e. the deviation of the real position $s(t)$ from the ideal position $s_{\text{ideal}}(t)$ given by the control system.

In order to simplify the measurement of the drive dynamics, the values $n_{ij}$ in the pulse controller are set to a constant value $n$. Thus, the ideal position of the drive increases proportionally to the integral of the beam intensity $I(t)$:

$$s_{\text{ideal}}(t) = s^0 + \frac{20\ \mu\text{m}}{nf} \int_0^t I(t')\,\mathrm{d}t' \tag{3}$$

where the beam intensity $I(t)$ is defined as the particle rate of the beam and $f$ is defined as in section (2.2.3). In the same manner the ideal velocity of the drive can be written as

$$v_{\text{ideal}}(t) = \frac{20\ \mu\text{m}}{nf} I(t). \tag{4}$$

Using a linear encoder (Heidenhain, Germany) with a resolution of 1 $\mu$m and a Lecroy 400 MHz digital oscilloscope for the fast sampling of the encoder signals we measured the real velocity $v(t)$ of the drive in comparison with the ideal velocity (beam intensity).

Figure 6 shows the typical behaviour of the drive for a fractional time interval of a depth scan. Due to the strong fluctuations of the beam intensity the ideal velocity $v_{\text{ideal}}(t)$ has phases of high positive and negative acceleration. The drive easily reaches the required acceleration values but shows a small overshoot. However, this overshoot is so small, that for normal scanning conditions the deviation $\Delta s(t) = \int (v_{\text{ideal}} - v)\,\mathrm{d}t$ from the ideal position is always smaller than 200 $\mu$m (see the lower part of figure 6), which guarantees the desired accuracy in dose (3%) for the superposition of the Bragg curves.

### *3.2. Production of spread-out Bragg peaks*

In order to prove the feasibility of depth scanning, we measured the depth dose distribution of spread-out Bragg peaks produced with the depth scanner. For instance a dose profile with an extension of the high dose area from 100 to 140 mm depth was produced using a 270 MeV $u^{-1}$ $^{12}C$ beam (see figure 7). With a single extraction phase (spill) of 2 s length the complete spread-out Bragg peak was produced. Repeating this scan many times, the depth dose in water was measured with another parallel plate ionization chamber and a water column of variable thickness, that was changed stepwise after each scan (Schardt 1993). The measurement was repeated five times and the points from the different measurements were nearly identical ($\Delta D < 1\%$), proving the excellent reproducibility of the system.

Because the time structure $I(t)$ of a synchrotron beam is always different from spill to spill, the $v(t)$ function of the drive is different as well, but the result for repeated depth scans has to be the same. Therefore, the good reproducibility of the resulting depth dose profile proves the high quality of the depth scanning system. Figure 7 also shows good agreement with the planned depth dose distribution. The small deviation at the distal end of the extended Bragg peak is also found in comparable measurements using the lateral raster-scan system and is due to the physical beam model (Krämer *et al* 2000) actually used.

### *3.3. Scanning in three dimensions and dose verification*

As described in section 2.1.1 the depth scanner is designed for three-dimensional conformal irradiation of arbitrarily shaped target volumes. In a first trial we produced a dose distribution with a spherical volume of high dose and a sharp dose fall-off at the border of the sphere. Using a 270 MeV $u^{-1}$ $^{12}C$ beam from the GSI synchrotron the sphere with a diameter of 5 cm was filled with a series of 121 different cylindrical spread-out Bragg peaks shifted in the transversal direction. The cylinders were grouped in 11 planes having 3 to 14 cylinders. The displacement from plane to plane was realized by moving the target vertically, whereas the change from cylinder to cylinder was performed by a stepwise rotation of the target, which should simulate the rotation of the gantry (see also figure 3). In order to avoid problems with singularities in the centre of rotation, the centre was placed far outside of the target volume (bottom left at the border of the measured volume in figure 8). The diameter of the beam was adjusted to 7 mm (FWHM), guaranteeing sufficient transverse overlap of the cylinders for a smooth dose distribution. The total irradiation took about 6 minutes and produced a dose of 10 Gy in the target volume.

For dose verification we used NMR imaging of water equivalent BANG$^{TM}$ gels (Maryanski *et al* 1993), a new technique in 3D heavy ion dosimetry (Ramm *et al* 1999). A bottle filled with a BANG polymer gel was mounted as target on the depth scanner. The irradiation causes local changes in the molecular structure of the BANG gel and changes the longitudinal and transversal relaxation time $T_1$ and $T_2$ of the water protons. The changes are large enough to be mapped by an NMR scanner (Magnetom, Siemens) with high resolution of 1 mm. The transverse relaxation rate $R_2 = 1/T_2$ was used as a measure of the absorbed dose. Due to saturation effects in the high LET tracks of heavy ions the deposited dose $D(x, y, z)$ is not exactly proportional to the relaxation rate $R_2(x, y, z)$. The exact calibration of the dose in the mixed field of a heavy ion spread-out Bragg peak is the subject of a separate project (Ramm *et al* 2000), but in this experiment with the depth scanner we were mainly interested in verifying the spatial shape of the target volume filled with high dose, the dose fall-off at the border and the dose homogeneity in the target volume. The exact verification of dose values has already been performed with the water column for the one-dimensional case (see section 3.2).

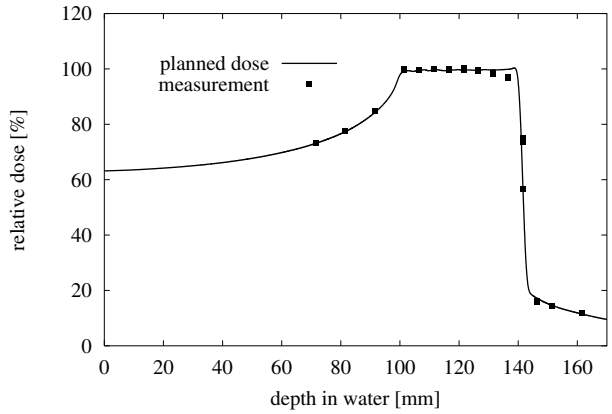


**Figure 7.** Measured depth–dose profile in comparison to the planned dose.

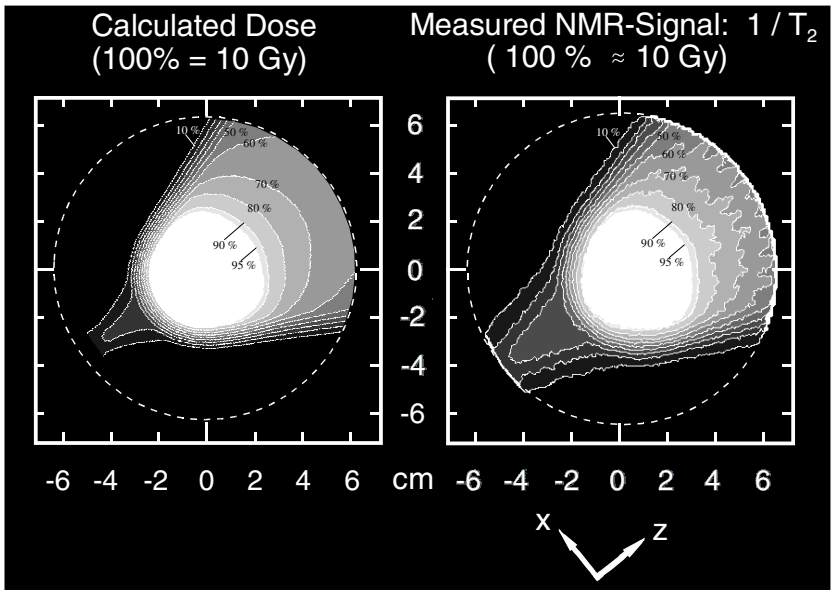


**Figure 8.** Dose distribution over the middle plane of a spherical target volume. The left diagram shows the dose calculated from the planning in comparison with the $1/T_2$ relaxation time in a BANG$^{TM}$ gel measured with an NMR scanner (right side). The quantity $T_2^{-1}(x, y, z)$ is in first order proportional to the deposited dose $D(x, y, z)$.

Figure 8 shows the $1/T_2$-distribution over the mid plane of the irradiated sphere in comparison to the planned dose. For the planning of the 3D depth scan the material (glass) and the geometry of the BANG gel bottle were taken into account meticulously. At the right side of the target volume the measured dose shows a small inhomogeneity (ripples in the isodose lines) caused by a beam which had a diameter slightly smaller than planned. Therefore, the overlap outside of the target volume was not sufficient for an absolutely smoothed dose distribution. However, the measured and the planned dose distribution agree very well with each other.

### *3.4. Treatment planning with depth scanning*

In order to estimate the duration of patient irradiation with depth scanning, some treatment plans were produced taking as basis typical treatment plans of patients who had been treated with the GSI raster scanning system in July/August 2000.

In table 1 the percentage of interrupted iso-energy slices for raster scanning is compared with the percentage of interrupted cylinders for depth scanning. The interruptions in the beam's path in the slices or in the cylinders respectively are caused by an irregular shape of the tumour or by the inhomogeneous density in the body. As was explained in section 1, the percentage of interruptions for depth scanning is much smaller than for raster scanning (compare columns 4 and 7).

Furthermore, the irradiation times for raster scanning and those for depth scanning are compared. Using the same beam diameter as for raster scanning at GSI (4–7 mm FWHM), the treatment time for depth scanning is much longer than for raster scanning (compare columns 5 and 8). However, using a beam diameter of 10 mm—as is usually done in proton therapy with beam scanning—the number of columns and the irradiation time can be reduced by a factor of four (column 9). On the other hand an increased beam width causes a less sharp dose fall-off at the border of the target. This will be discussed in section 4.

## 4. Summary and discussion

Depth scanning represents a novel technique to achieve a three-dimensional irradiation of an individual target volume. Generally, the scanning procedure for lateral scanning and for depth scanning as well is to compensate the intensity fluctuations in time of the extracted beam and to produce a smooth superposition of ion beams. In principle, the only difference between the two techniques is the chronology for the superposition of the particle beams. Both techniques can yield the same conformity in dose.

A disadvantage of the depth scanning system is that it is slower than the lateral magnetic deflection system, because there is only one dimension that can be covered very fast (see section 3.4). An increased beam diameter would drastically reduce the irradiation time for depth scanning. The resulting loss of sharpness of the dose fall-off could be compensated in many cases with an optional collimator, that shields critical parts of the normal tissue (e.g. the double-leaf collimator of the PSI facility (Pedroni *et al* 1995)). At a proton beam facility the unavoidable scattering (at the exit window, the beam monitors and in the patient) induces a minimum beam width of roughly 10 mm FWHM. Here, depth scanning would guarantee an acceptable treatment time with an optimal dose fall-off for proton beams.

On the other hand the lateral scanning has the disadvantage that first, a sophisticated and consequently expensive control system is necessary and second, the density inhomogeneities in front of and in the target volume destroy a linear correspondence between particle energy and range and result in complex irradiation patterns.

Depth scanning is the attempt to transfer the scanning advantages, i.e. the feedback between extracted intensity and dose deposition, into the longitudinal direction, which seems to be more adequate to the problem of density correlated range variations. A gantry system with a depth scanner would have a lower weight than a gantry with a raster scanner due to the smaller aperture of the last bending magnet.

This first paper reports on the technical feasibility of the depth scanning concept. The experiments have shown that even for the fluctuating intensity of a synchrotron beam a mechanical compensation is possible using a set of wedges mounted on a linear motor rail.

**Table 1.** Irradiation times for lateral scanning in comparison to depth scanning. Four typical treatment plans (with two to four fields per plan) for the GSI raster scan device have been selected for this table. The maximum lateral extension (in a beams eye view) of the fields is given in column 2. Column 3 shows the number of energy steps for the raster scanning. The percentage of interrupted iso-energy slices is shown in column 4. The irradiation time (column 5) is the recorded start–stop time averaged over all fractions (mostly 20 fractions). In order to calculate a theoretical irradiation time for depth scanning, plans for depth scanning (see section 2.1) were calculated that produce the same theoretical dose distributions as the fields for raster scanning. Column 6 contains the number of cylinders ($N_i$) of these plans. The percentage of interrupted cylinders is given in column 7. Supposing that two cylinders per spill period (≈5 s) can be processed, the irradiation time in column 8 was directly calculated from column 6. Using a beam diameter of 10 mm FWHM the number of cylinders and the irradiation time (column 9) can be reduced by a factor of four.

| | | Raster scanning | | | Depth scanning | | | |
|---|---|---|---|---|---|---|---|---|
| Patient (field) | Lateral extension of the tumour [cm] | Number of energies | Interrupted slices [%] | Irradiation time [min] | Number of cylinders | Interrupted cylinders [%] | Irradiation time (beam width 5 mm) [min] | Irradiation time (beam width 10 mm) [min] |
| P61 a | 8 | 57 | 18 | 9.00 | 905 | 3 | 37 | 9 |
| b | 8 | 54 | 6 | 8.00 | 953 | 4 | 40 | 10 |
| c | 3 | 12 | 14 | 2.00 | 502 | 0 | 21 | 5 |
| d | 4 | 23 | 8 | 3.00 | 811 | 5 | 34 | 9 |
| P65 a | 6 | 42 | 6 | 6.00 | 508 | 3 | 21 | 5 |
| b | 6 | 40 | 9 | 5.30 | 491 | 1 | 20 | 5 |
| c | 3 | 9 | 10 | 1.30 | 532 | 0 | 22 | 5 |
| P66 a | 8 | 46 | 6 | 6.00 | 573 | 5 | 24 | 6 |
| b | 9 | 39 | 9 | 6.00 | 592 | 2 | 24 | 6 |
| P67 a | 8 | 28 | 17 | 5.30 | 871 | 3 | 36 | 9 |
| b | 8 | 30 | 21 | 5.30 | 913 | 2 | 38 | 9 |
| c | 3 | 10 | 44 | 2.30 | 579 | 0 | 24 | 6 |

The acceleration of such a system is fast enough to follow the intensity fluctuations with high precision. The experiments with ionization chambers as well as the 3D irradiation of a BANG gel demonstrate the technical feasibility of such a system and its high precision.

The fast absorber system of the depth scanner could replace the modulator wheels and ridge filters in standard ion therapy facilities (without scanning) and has the advantage that it is no longer necessary to exchange these modulators for different depth–dose profiles.

Furthermore, in existing therapy units in which the lateral displacement of the dose can be achieved by gantry motion and a gentle move of the patient, the insertion of a depth scanning system is an easy way to achieve three-dimensional target conformal irradiation with only minor changes of the control system.

Consequently, the depth scanning system is an alternative to lateral scanning. Depth scanning with proton beams can be used to irradiate many types of tumour. For example, tumours with an extension up to 10 cm can be irradiated within 5–10 min, as shown in table 1. Using the sharper heavy ion beams, depth scanning is ideal for the treatment of small target volumes (radio surgery) that can be irradiated in a short time.

## Acknowledgments

The authors thank Dr Ulla Ramm (Uni-Klinik Frankfurt) and Dr Michael Bock (DKFZ Heidelberg) for their help in NMR analysis of the BANG gels. We also thank Dr Dieter Schardt (GSI Darmstadt) for his support in measuring depth–dose profiles.

## References

Badura E *et al* 2000 Control system for cancer therapy with a heavy ion beam at GSI *IEEE Trans. Nucl. Sci.* **47** 170–3

Chu W, Ludewigt B and Renner T 1993 Instrumentation for treatment of cancer using proton and light-ion beams *Rev. Sci. Instrum.* **64** 2055–122

Debus J *et al* 2000 Fractionated carbon ion irradiation of skull base tumours at GSI—first clinical results and future perspectives *Strahlenther. Onkol.* **176** 211–6

Dreifke L 1997 Effektive Automatisierung durch parallele Antriebssysteme *Booklet of Company DPS Direktantriebe D-98529 Suhl*

Goitein M 1983 Beam scanning for heavy charged particle radiotherapy *Med. Phys.* **10** 831–40

Groß K *et al* 1998 Proposal for a dedicated ion beam facility for cancer therapy GSI Darmstadt

Haberer T, Becher W, Schardt D and Kraft G 1993 Magnetic scanning system for heavy ion therapy *Nucl. Instrum. Methods* A **330** 296–314

Jacob C 1997 Reichweite CT-Zahl Beziehung von Phantommaterialien *PhD Thesis* Universität Heidelberg p 50

Jongen Y, Beeckman W and Laisné A 1991 A development of a low-cost compact cyclotron system for proton therapy *Proc. NIRS Int. Workshop on Heavy Charged Particle Therapy and Related Subjects* NIRS-M-81, pp 189–200

Krämer M, Jäckel O, Haberer T, Kraft G, Schardt D and Weber U 2000 Treatment planning for heavy-ion radiotherapy: physical beam model and dose optimization *Phys. Med. Biol.* **45** 3299–317

Kraft G 1998 Radiotherapy with heavy ions: radiobiology, clinical indications and experience at GSI, Darmstadt *Tumori* **84** 200–4

Kraft G and Weber U 1998 Bestrahlungssystem mit intensitätsgesteuerter Tiefenmodulation zur volumenkonformen Bestrahlung von tiefliegenden Tumouren mit Protonen und leichten Ionen *Patent Pending* Deutsch. Patentamt Az. 19907098.9, European Patent Office 00/01149

Maryanski M, Gore J, Kennan R and Schulz R 1993 NMR relaxation enhancement in gels polymerised and cross-linked by ionizing radiation: a new approach to 3D dosimetry by MRI *Magn. Reson. Imaging* **11** 253–8

Pavlovic M 1997 Beam-optics study of the gantry beam delivery system for light-ion cancer therapy *Nucl. Instrum. Methods* A **399** 439–54

Pedroni E *et al* 1995 The 200 MeV proton therapy project at the Paul Scherrer Insitute: cnceptual design and practical realisation *Med. Phys.* **22** 37–53

Ramm U *et al* 1999 3D Heavy ion dosimetry using BANG polymer-gel and magnetic resonance imaging *GSI Scientific Report* 1998 GSI-99-1, p 132

Ramm U, Weber U, Bock M, Krämer M, Bankamp A, Damrau M, Thilmann C, Böttcher H, Schad L and Kraft G 2000 Three-dimensional BANG$^{TM}$ gel dosimetry in conformal heavy ion radiotherapy *Phys. Med. Biol.* **45** N95–N102
Schardt D 1993 Bragg curve measurements with ionisation chambers *GSI Scientific Report* 1992 GSI-93-1, p 336